

REPORT DOCUMENTATION PAGEForm Approved
OMB No. 074-0188

Public reporting burden for this collection of information is estimated to average 1 hour per response, including the time for reviewing instructions, searching existing data sources, gathering and maintaining the data needed, and completing and reviewing this collection of information. Send comments regarding this burden estimate or any other aspect of this collection of information, including suggestions for reducing this burden to Washington Headquarters Services, Directorate for Information Operations and Reports, 1215 Jefferson Davis Highway, Suite 1204, Arlington, VA 22202-4302, and to the Office of Management and Budget, Paperwork Reduction Project (0704-0188), Washington, DC 20503

1. AGENCY USE ONLY (Leave blank)		2. REPORT DATE 1996	3. REPORT TYPE AND DATES COVERED Progress Report, July 1996	
4. TITLE AND SUBTITLE Study of the Spatial Structure of Arctic Ocean Variability			5. FUNDING NUMBERS Subcontract No. 4500033242	
6. AUTHOR(S) N.G. Yakovlev, A.S. Sarkisyan, & S.V. Pisarev				
7. PERFORMING ORGANIZATION NAME(S) AND ADDRESS(ES) Marine Science International Corporation			8. PERFORMING ORGANIZATION REPORT NUMBER MSIC Report No. 3/96	
9. SPONSORING / MONITORING AGENCY NAME(S) AND ADDRESS(ES) SERDP 901 North Stuart St. Suite 303 Arlington, VA 22203			10. SPONSORING / MONITORING AGENCY REPORT NUMBER N/A	
11. SUPPLEMENTARY NOTES This work was supported in part by SERDP under Subcontract No. 4500033242. The United States Government has a royalty-free license throughout the world in all copyrightable material contained herein. All other rights are reserved by the copyright owner.				
12a. DISTRIBUTION / AVAILABILITY STATEMENT Approved for public release: distribution is unlimited			12b. DISTRIBUTION CODE A	
13. ABSTRACT (Maximum 200 Words) There were three directions to this study-theoretical modeling, collection and systemization of experimental data, and analysis of long-term variations in the Arctic Basin. The work with the experimental data included: 1. The creation of a new version of the Arctic basin Data Base. 2. The collection & preliminary analysis of the archive data on the water exchange through the Fram Strait... 3. A comparison of the heat content variability in the Atlantic layer in different oceanographic regions.... 4. A comparison of salinity variations in the upper ocean layers in these regions.				
14. SUBJECT TERMS SERDP, Long-term variations, Arctic Basin			15. NUMBER OF PAGES 23	
			16. PRICE CODE N/A	
17. SECURITY CLASSIFICATION OF REPORT unclass.	18. SECURITY CLASSIFICATION OF THIS PAGE unclass.	19. SECURITY CLASSIFICATION OF ABSTRACT unclass.	20. LIMITATION OF ABSTRACT UL	

NSN 7540-01-280-5500

Standard Form 298 (Rev. 2-89)
Prescribed by ANSI Std. Z39-18
298-102

DTIC QUALITY INSPECTED 1

19980709 114

MARINE SCIENCE INTERNATIONAL CORPORATION

STUDY OF THE SPATIAL STRUCTURE OF ARCTIC OCEAN VARIABILITY

PROGRESS REPORT

Subcontract NO. 4500033242

N.G. Yakovlev
A.S. Sarkisyan
(Section I)

S.V. Pisarev
(Section II)

MSIC Report No. 3/96

1996

STUDY OF THE SPATIAL STRUCTURE OF ARCTIC OCEAN VARIABILITY

PROGRESS REPORT

N.G. Yakovlev
A.S. Sarkisyan
(Section I)

S.V. Pisarev
(Section II)

ABSTRACT

There were three directions to this study- theoretical modeling, collection and systematization of experimental data, and analysis of long-term variations in the Arctic Basin. The work with the experimental data included:

1. The creation of a new version of the Arctic Basin Data Base by combining the WOA-94, MOODS, and the historical Russian data. The data base will be used for studying the evolution of large-scale thermohaline anomalies, as well as further development of the theoretical model.
2. The collection and preliminary analysis of the archive data on the water exchange through Fram Strait and the runoff of the Siberian rivers as important factors influencing the oceanographic and ice conditions in the Arctic Ocean. (These data will be used later for modeling of the Arctic Ocean response to external impacts).
3. A comparison of the heat content variability in the Atlantic layer in different oceanographic regions outlined in the report "Climatic variability of the Arctic ocean" (Final report, MSIC, 1996).
4. A comparison of salinity variations in the upper ocean layers in these regions.

The aim of the theoretical work was to improve the numerical scheme for modeling the Atlantic water inflow into the Arctic Basin, and was performed by N.G. Iakovlev. The results of the modeling are described in Section I of the Report.

A description of the new version of the Arctic Basin Data Base is presented in Section II.

TABLE OF CONTENTS

	page
I. NUMERICAL MODELING OF THE ARCTIC OCEAN RESPONSE TO EXTERNAL FORCING	4
1.1. The development of the new numerical scheme	4
1.1.1. Rationale	4
1.1.2. New formulation of the general circulation model	4
1.1.3. The new time scheme	8
1.1.4. Results and problems	9
1.2. Comments on the choice of turbulent mixing/diffusion coefficients	17
II. THE CURRENT VERSION OF THE ARCTIC BASIN OCEANOGRAPHIC DATA BASE	18
2.1. Introduction	18
2.2. The new version of CTD data in the Arctic part of the WOA-94	18
2.3. The preliminary results of merging the Arctic Master Oceanographic Observation Data Set and the World Ocean Atlas -1994	20
2.4. The current composition of the Arctic Basin Data Base	21
REFERENCES	23

LIST OF FIGURES

	page
Fig. 1.1. Flow velocity at 250m for the nonslip boundary condition	10
Fig. 1.2. Flow velocity at 250m for the slip condition	11
Fig. 1.3. Flow velocity at the 25m depth	13
Fig. 1.4. Flow velocity at the 500m depth	14
Fig. 1.5. Test for the velocity oscillation at the side boundary	15
Fig. 1.6. Flow velocity averaged over four grid points	16

LIST OF TABLES

	page
Table 1.1. The coefficients of horizontal mixing in different models	17
Table 2.1. The distribution of the profiles of the CD-ROM "Replacement CTD data - 96" and the WOA-94	19
Table 2.2. The distribution of the profiles from the MOODS and the WOA-94	20
Table 2.3. Miscellaneous information about the current Arctic Basin Data Base	21-23

I. ON NUMERICAL MODELING OF THE ARCTIC OCEAN RESPONSE TO EXTERNAL FORCING

1. 1. The development of the new numerical scheme

1.1.1. Rationale

One of the prominent features of the water circulation in the Arctic Ocean is the existence of narrow coastal jets, one of which is the West Spitsbergen current supplying the Arctic with warm Atlantic water. In the previous version of our general ocean circulation model, this current was almost absent because of comparatively low spatial resolution and nonslip boundary conditions for the velocity components at the side boundary, and at the bottom. The width of the Fram Strait is about 400 km, i.e. ~ four grid steps. To allow for the Atlantic water inflow we had to specify a model of the bottom bathymetry deeper than that in reality, thus making it necessary for us to develop a new numerical scheme.

The first, direct, way to improve the simulation of the coastal jets is to refine both the horizontal and vertical spatial discretization. This demands no changes in computer programming and, at first glance, may seem very attractive. However, even when we choose a grid size three times smaller, it barely allows us to get results on the circulation sensitivity in reasonable "real" time. Moreover, the nonslip boundary condition for the velocity is acceptable only when the grid size is much less than the internal Rossby radii - for the Arctic, it is about 10 km, i.e., 10 times less than the grid size used in the model.

The second way is to design a special coordinate system refining the areas of interest. The simplest versions of this approach have been proposed by S. Hakkinen (USA) and by G. Semjonov (AARI, Russia). The approach is fine, but, unfortunately, the area considered changes in time.

We decided to change the boundary conditions and assume conditions with free slip at the side boundary and quadratic friction at the bottom. This approach does not contradict the first and second approaches, but may even complement them, if necessary.

1.1.2. New formulation of the general circulation model

The basic features of the new model are the same as in the previous version, but the boundary conditions for the horizontal components of the velocity are different.

Let us consider the system of equations of large-scale ocean dynamics under commonly used assumptions in a 3D area Ω bounded by plane $z=0$ and sufficiently smooth bottom topography $z=H(x, y)$. To simplify the presentation, we use the Cartesian coordinate system (x, y, z) .

$$\begin{aligned}\frac{\partial u}{\partial t} + Lu - lv &= -\frac{1}{\rho_0} \frac{\partial P}{\partial x} + Du \\ \frac{\partial v}{\partial t} + Lv + lu &= -\frac{1}{\rho_0} \frac{\partial P}{\partial y} + Dv \\ \frac{\partial P}{\partial z} &= \rho g\end{aligned}$$

$$\frac{\partial u}{\partial x} + \frac{\partial v}{\partial y} + \frac{\partial w}{\partial z} = 0 \quad (1)$$

$$\frac{\partial T}{\partial t} + LT = D_T T$$

$$\frac{\partial S}{\partial t} + LS = D_S S$$

$$\rho = \rho(T, S)$$

Here u, v, w are the components of the velocity \mathbf{u} along the axes x, y, z respectively, P is the pressure, T, S are the temperature and the salinity, ρ is the density anomaly compared with the constant ρ_0 , l is the Coriolis parameter, g is the gravity acceleration, and t is time. L, D, D_T, D_S are the operators of advection, turbulent mixing of momentum, and turbulent diffusion of heat and salt, respectively.

We specify the advection as

$$L\phi = \frac{\partial}{\partial x} u\phi + \frac{\partial}{\partial y} v\phi + \frac{\partial}{\partial z} w\phi,$$

and turbulent mixing and diffusion as

$$D\phi = \frac{\partial}{\partial z} v \frac{\partial \phi}{\partial z} + \frac{\partial}{\partial x} \mu \frac{\partial \phi}{\partial x} + \frac{\partial}{\partial y} \mu \frac{\partial \phi}{\partial y},$$

$$D_\phi \phi = \frac{\partial}{\partial z} v_\phi \frac{\partial \phi}{\partial z} + \frac{\partial}{\partial x} \mu_\phi \frac{\partial \phi}{\partial x} + \frac{\partial}{\partial y} \mu_\phi \frac{\partial \phi}{\partial y}.$$

Let the boundary consist of two parts: $\Gamma = \Gamma_0 \cup \Gamma_1$, where Γ_1 is a "liquid" boundary (passages and rivers). As for the first part of the boundary, let $\Gamma_0 = \Gamma_s \cup \Omega_0$, where Ω_0 is an intersection of $\bar{\Omega}$ with the plane $z=0$, and Γ_s is a "solid" boundary representing the land.

Let the boundary conditions for momentum be as follows:

$$\begin{aligned} \nu \rho_0 \frac{\partial u}{\partial N} = \tau^{(x)}, \quad \nu \rho_0 \frac{\partial v}{\partial N} = \tau^{(y)} \quad \text{on } \Gamma_0, \\ u_n = 0 \quad \text{on } \Gamma_s, \\ w = \frac{\partial \zeta}{\partial t} \quad \text{on } \Omega_0, \\ u = u_b, \quad v = v_b \quad \text{on } \Gamma_1. \end{aligned} \quad (2)$$

For temperature and salinity we specify the following boundary conditions:

$$\begin{aligned} \frac{\partial T}{\partial N_T} = Q_T, \quad \frac{\partial S}{\partial N_S} = Q_S \quad \text{on } \Gamma_0, \\ T = T_b, \quad S = S_b \quad \text{on } \Gamma_1. \end{aligned}$$

Here $\zeta(x, y, t) = \frac{l}{\rho_0 g} P(x, y, 0, t)$ is the sea surface elevation, n is the outer normal vector, u_n is

the velocity component along the vector n , $\frac{\partial}{\partial N} = \mu \frac{\partial}{\partial x} \cos(n, x) + \mu \frac{\partial}{\partial y} \cos(n, y) + \nu \frac{\partial}{\partial z} \cos(n, z)$

is the conormal derivative corresponding to the momentum turbulent mixing. Derivatives $\frac{\partial}{\partial N_T}$

and $\frac{\partial}{\partial N_S}$ are specified in the same way. Functions $\tau^{(x)}, \tau^{(y)}$, u_b , v_b , T_b , S_b , Q_T , and Q_S are assumed to be known.

The initial conditions at $t=0$ are as follows:

$$u = u^{(0)}, v = v^{(0)}, T = T^{(0)}, S = S^{(0)} \text{ and } \zeta = \zeta^{(0)}.$$

Note 1. In general, the linearized kinematic condition $w = \frac{\partial \zeta}{\partial t}$ on $z=0$ is valid for $\zeta \ll H$.

This condition is not satisfied in the vicinity of $\Gamma_s \cap \Omega_0$. However, in a discrete model, after applying the finite element technique, we find $\min H(x,y) \approx 10m$, while the scale of level variations is about $1m$.

To develop a finite element scheme we pose a projection form of the problem (1)-(2), where functions $\pi_1, \pi_2, \pi_T, \pi_S \in W_2^1(\Omega)$ are equal to zero on Γ_1 , and functions $\pi_3, \pi_4, \pi_\rho \in W_2^1(\Omega)$:

$$\begin{aligned} \left(\frac{\partial u}{\partial t}, \pi_1\right) - B(u, \mathbf{u}, \pi_1) - (lv, \pi_1) &= -\frac{1}{\rho_0} \left(\frac{\partial P}{\partial x}, \pi_1\right) - [u, \pi_1] + f_1, \\ \left(\frac{\partial v}{\partial t}, \pi_2\right) - B(v, \mathbf{u}, \pi_2) + (lu, \pi_2) &= -\frac{1}{\rho_0} \left(\frac{\partial P}{\partial y}, \pi_2\right) - [v, \pi_2] + f_2, \\ \left(\frac{\partial P}{\partial z}, \pi_3\right) &= (\rho g, \pi_3), \\ -\left(u, \frac{\partial \pi_4}{\partial x}\right) - \left(v, \frac{\partial \pi_4}{\partial y}\right) - \left(w, \frac{\partial \pi_4}{\partial z}\right) &= f_3, \\ \left(\frac{\partial T}{\partial t}, \pi_T\right) - B(T, \mathbf{u}, \pi_T) &= -[T, \pi_T]_T + f_T, \\ \left(\frac{\partial S}{\partial t}, \pi_S\right) - B(S, \mathbf{u}, \pi_S) &= -[S, \pi_S]_S + f_S, \\ (\rho, \pi_\rho) &= (\rho(T, S), \pi_\rho). \end{aligned}$$

The following denotations are used here:

$$\begin{aligned} (a, b) &= \int_{\Omega} abd\Omega, \\ B(a, \mathbf{u}, b) &= \int_{\Omega} \left(au \frac{\partial b}{\partial x} + av \frac{\partial b}{\partial y} + aw \frac{\partial b}{\partial z} \right) d\Omega, \\ [a, b] &= \int_{\Omega} \left(\mu \frac{\partial a}{\partial x} \frac{\partial b}{\partial x} + \mu \frac{\partial a}{\partial y} \frac{\partial b}{\partial y} + \nu \frac{\partial a}{\partial z} \frac{\partial b}{\partial z} \right) d\Omega, \end{aligned}$$

and $[a, b]_a$ is specified in similar way. The right-hand sides f_1, f_2, f_3, f_T , and f_S are generated by boundary conditions.

As in the previous version of the model, we choose right triangular prisms to be the finite elements. Let the bases of the prisms lie on the planes $z = z_k$, $k = 1, \dots, K_0$, and the vertexes of the prisms belong to the set of points $P_i(x, y), i = 1, \dots, M$. Let each index i correspond to the

integer number $KL(i) \leq K_0$, hence $z_{KL(i)}$ will be treated as a depth at point $P(i)$. On the finite elements, we specify the basis functions $\pi_{i,k} = \varphi_i(x,y)\psi_k(z)$, where $\varphi_i(x,y)$ are 2D finite linear piecewise functions defined on triangular finite elements and $\psi_k(z)$ are 1D finite linear piecewise functions, so called "the roofs" (Marchuk and Agoshkov, 1981; Zienkiewicz, 1977). The approximate solution is represented by sums of the form $\Phi^h = \sum_{i,k} \Phi_{i,k} \pi_{i,k}$. Probe functions

$\pi_i, i=1, \dots, 4, \pi_T, \pi_S, \pi_p$ are also chosen among $\pi_{i,k}$. The vector of coefficients $\Phi_{i,k}$ will be denoted by

$$\bar{\Phi} = (\Phi_{1,1}, \dots, \Phi_{1, KL(1)}, \Phi_{2,1}, \dots, \Phi_{2, KL(2)}, \dots, \Phi_{M, KL(M)})^T.$$

It is obvious, that ζ^h is approximated by the sum of $\varphi_i(x,y)$.

We constantly apply the so called "lumping-method" to derive the system of ordinary differential equations for vectors $\bar{u}, \bar{v}, \bar{w}, \bar{P}, \bar{T}, \bar{S}, \bar{p}, \bar{\zeta}$. Instead of Gram matrix G for functions $\pi_{i,k}$ we use the diagonal matrix M with the elements

$$(M)_{(i,k),(l,m)} = \delta_{(i,k),(l,m)} \int_{\Omega^h} \pi_{i,k} d\Omega^h,$$

$$\text{where } \delta_{(i,k),(l,m)} = \begin{cases} 1, & \text{if } i = l \text{ and } k = m \\ 0, & \text{if } i \neq l \text{ or } k \neq m \end{cases}.$$

The Gram matrix G_1 for functions $\pi_{i,k}$ in a space with the scalar product weighted by l_i is substituted for the diagonal matrix C with the elements

$$(C)_{(i,k),(l,m)} = \delta_{(i,k),(l,m)} l_i \int_{\Omega^h} \pi_{i,k} d\Omega^h.$$

The gradient approximation is defined by the formulae:

$$(\nabla_x^h \bar{P})_{i,k} = \int_{\Omega^h} \left(\sum_{l=1}^M P_{l,k} \frac{\partial \varphi_l}{\partial x} \right) \pi_{i,k} d\Omega^h,$$

$$(\nabla_y^h \bar{P})_{i,k} = \int_{\Omega^h} \left(\sum_{l=1}^M P_{l,k} \frac{\partial \varphi_l}{\partial y} \right) \pi_{i,k} d\Omega^h,$$

$$(\nabla_z^h \bar{P})_{i,k} = \int_{\Omega^h} \left(\sum_{m=1}^{KL(i)} P_{l,k} \frac{\partial \psi_m}{\partial z} \right) \pi_{i,k} d\Omega^h.$$

The trilinear form B is approximated according to the formula:

$$- \int_{\Omega^h} u \varphi^h \frac{\partial \varphi_i}{\partial x} \psi_k d\Omega^h \approx - \int_{\Omega^h} \left(\sum_{m=1}^M u_{m,k} \varphi_m \right) \left(\sum_{l=1}^M \varphi_{l,k} \varphi_l \right) \frac{\partial \varphi_i}{\partial x} \psi_k d\Omega^h,$$

and the two rest terms are approximated in a similar way. The matrix approximation of B will be denoted as A . Applying the lumping method for the turbulent mixing/diffusion operators, we obtain the matrices D, D_T and D_S derived with the use of the approximate equality

$$\int_{\Omega^h} \mu \frac{\partial \phi^h}{\partial x} \frac{\partial \varphi_i}{\partial x} \psi_k d\Omega^h \approx \int_{\Omega^h} \mu \left(\sum_{l=1}^M \phi_{l,k} \frac{\partial \varphi_l}{\partial x} \right) \frac{\partial \varphi_i}{\partial x} \psi_k d\Omega^h$$

(and the same for the last terms). The coefficients of turbulent mixing/diffusion are assumed to be constant over a finite element.

As a result we have the following system of ordinary differential equations:

$$\begin{aligned} \mathbf{M} \frac{d\bar{u}}{dt} + \mathbf{A}\bar{u} - \mathbf{C}\bar{v} &= -\frac{1}{\rho_0} \nabla_x^h \bar{P} + \mathbf{D}\bar{u} + \bar{f}_1, \\ \mathbf{M} \frac{d\bar{v}}{dt} + \mathbf{A}\bar{v} + \mathbf{C}\bar{u} &= -\frac{1}{\rho_0} \nabla_y^h \bar{P} + \mathbf{D}\bar{v} + \bar{f}_2, \\ \nabla_z^h \bar{P} &= g\mathbf{M} \bar{\rho}, \\ -(\nabla_x^h)^T \bar{u} - (\nabla_y^h)^T \bar{v} - (\nabla_z^h)^T \bar{w} &= \bar{f}_3, \\ \mathbf{M} \frac{d\bar{T}}{dt} + \mathbf{A}\bar{T} &= \mathbf{D}_T \bar{T} + \bar{f}_T, \\ \mathbf{M} \frac{d\bar{S}}{dt} + \mathbf{A}\bar{S} &= \mathbf{D}_S \bar{S} + \bar{f}_S, \\ \bar{\rho} &= \bar{\rho}(\bar{T}, \bar{S}). \end{aligned} \quad (3)$$

1.1.3. The new time scheme

In the previously used version of the model, there was a time step limit stipulated by the Coriolis term approximation in time, and there was the explicit "leap-frog" scheme for the Coriolis force. According to the CFL criterion, one can conclude that the time step should not be greater than 1.9 hours. This limitation may turn out to be too severe, therefore the next step necessary to enhance the efficiency of the model is to change the Coriolis term time approximation. We used the Crank-Nicholson time approximation, so that

$$\mathbf{C}\bar{u} \approx \frac{1}{2} \mathbf{C}(\bar{u}^{j+1} + \bar{u}^{j-1}).$$

The new scheme leads to some additional difficulties which arise because the matrix for sea level was nonsymmetric, and the conjugate gradients method, used before, is no longer valid. The nonsymmetry is due to the method of deriving the matrix. To obtain the system of equations for $\bar{\zeta}^{j+1}$, we substitute \bar{u}^{j+1} , \bar{v}^{j+1} in the discrete integral continuity equation:

$$\begin{aligned} & -\frac{1}{\Delta t} (\zeta_i^{j+1} - \zeta_i^j) \int_{\Omega_0^h} \varphi_i d\Omega_0^h + \\ & + \int_{\Omega^h} ((u^h)^{j+1} \frac{\partial \varphi_i}{\partial x} + (v^h)^{j+1} \frac{\partial \varphi_i}{\partial y}) d\Omega^h = F_i, \quad i = 1, \dots, M \end{aligned}$$

which is derived from the discrete continuity equation by means of the summation over index k , taking into account the equality $\forall i \sum_{k=1}^{KL(i)} \psi_k(z) \equiv 1$. As a result, we have a system of linear algebraic equations with the positively defined matrix \mathbf{L} which satisfies the equation:

$$\begin{aligned}
(\mathbf{L}\bar{\zeta})_m = & \frac{1}{\Delta t} \zeta_m \int_{\Omega_0^h} \varphi_m d\Omega_0^h + g \int_{\Omega^h} [\sum_{i,k} \Delta_{i,k}^{-1} (\alpha a_{i,k} \int_{\Omega^h} \frac{\partial \zeta^h}{\partial x} \pi_{i,k} d\Omega^h + \\
& + \frac{1}{2} \alpha^2 b_{i,k} \int_{\Omega^h} \frac{\partial \zeta^h}{\partial y} \pi_{i,k} d\Omega^h) \pi_{i,k} \frac{\partial \varphi_m}{\partial x} + \\
& + \sum_{i,k} \Delta_{i,k}^{-1} (\alpha a_{i,k} \int_{\Omega^h} \frac{\partial \zeta^h}{\partial y} \pi_{i,k} d\Omega^h - \\
& - \frac{1}{2} \alpha^2 b_{i,k} \int_{\Omega^h} \frac{\partial \zeta^h}{\partial x} \pi_{i,k} d\Omega^h) \pi_{i,k} \frac{\partial \varphi_m}{\partial y}] d\Omega^h, \quad m = 1, \dots, M.
\end{aligned}$$

Here we use the denotations $\alpha = 2\Delta t$ for the "leap-frog" and $\alpha = \Delta t$ for the Matsuno time step,

$$a_{i,k} = \int_{\Omega^h} \pi_{i,k} d\Omega^h, \quad b_{i,k} = l_i a_{i,k}, \quad \Delta_{i,k} = a_{i,k}^2 + \alpha^2 b_{i,k}^2.$$

To solve the problem, we tested the Sequence Overrelaxation method (SOR), commonly used, and rather robust, and found, that for a time step greater than 1.0 hour, this method led to an underrelaxation (it converged only for a relaxation parameter of less than 1.0) and had too slow a convergence. If the time step is larger than 3.0 h, the SOR does not converge at all. For a time step of 1.0 h, the convergence of the method is quite acceptable for a relaxation parameter of 1.0.

We plan to examine the possibility of using the Generalized Minimal Residuals method (GMRES) with preconditioning. Where the matrix for sea level is time constant, all the necessary calculations of the preconditioning matrix and Krylov's subspace vectors need to be executed only once. We hope that the proper choice of the iteration method will allow us to use time steps of about 6 hours.

Note 2. For the implicit time approximation of vertical momentum turbulent mixing, the matrix for sea level is similar - only the right-hand side changes slightly. The implicit approximation may be very useful in the case of parameterization by Pacanowski and Philander (1981), when large vertical coefficients (up to $10^3 \text{ m}^2 \text{ s}^{-1}$) occur. In the case of an explicit time scheme, this will lead to extremely small time steps of about several minutes.

1.1.4. Results and Problems

As a test of the new numerical scheme, we carried out two sets of calculations. The first one was devoted to a comparison of the results of two models - with nonslip boundary conditions and with the new ones. We assumed that there was no wind, no rivers and no exchange through the passages. Our attention was focused on Fram Strait, rather than on the characteristics of the numerical model. The results are shown in Fig. 1.1 and Fig. 1.2. They show that our efforts were not in vain, and now the Atlantic water inflow looks more realistic, and, in addition, it can be seen that the overall circulation has become more intensive.

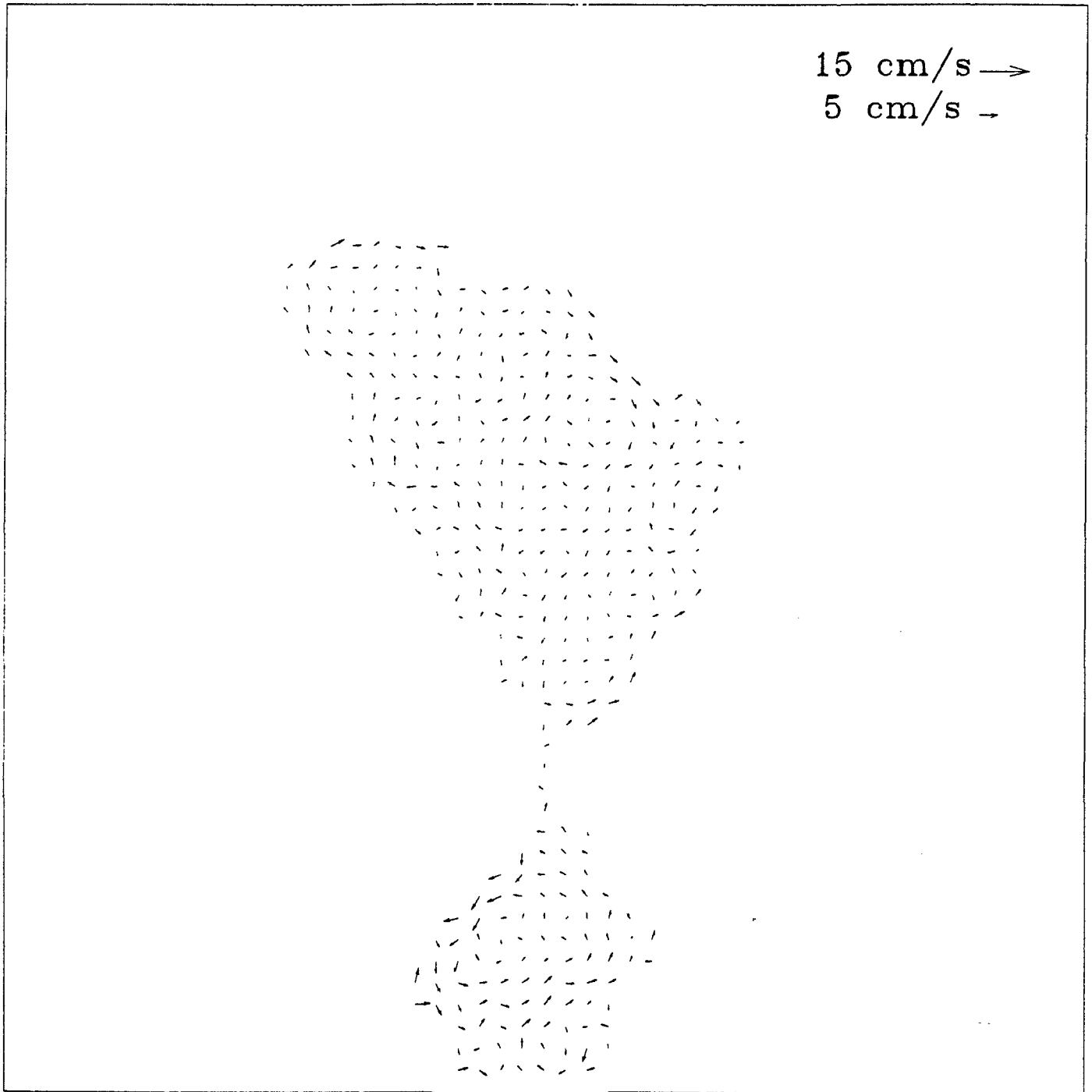


Fig. 1.1. Flow velocity at 250m for the nonslip boundary condition.

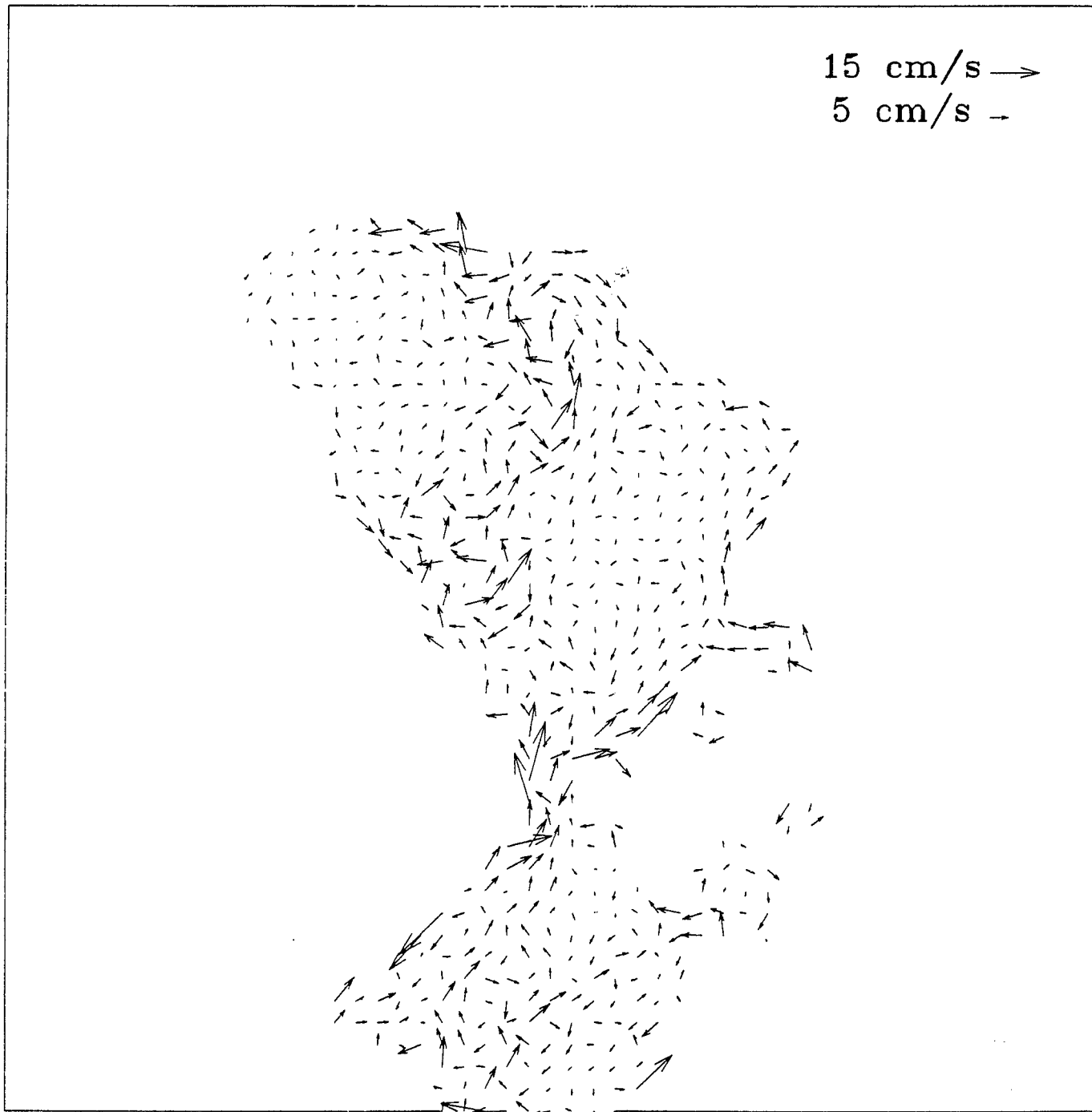


Fig. 1.2. Flow velocity at 250m for the slip condition.

The results of simulation of winter circulation specifying the wind stress and the water transport through the passages are shown in Fig. 1.3 and 1.4. Here we can see that there are very "noisy" velocity fields at the boundary, in the vicinity of relatively intensive currents, especially off Greenland and Scandinavia.

Some of the velocity vectors are directed opposite to the main currents (in the region of the East Greenland current, for example). This effect is very prominent in the upper layers (compare with Fig. 1.4 where the velocity field is rather smooth) and is located in the regions of strong Joint Effect of Baroclinicity and Bottom Topography (JEBAR, Sarkisyan, 1977). Note that this effect here is of numerical origin, and arises from the inconsistency of the bottom topography with the temperature/salinity fields used in the model. The T, S fields are rather smooth and, in the region of the East Greenland current, the isotherms and the isohalines follow almost parallel to the coast line. The bottom topography from the model, here, is in horizontal steps with sharp variations of depth from point to point and, hence, the opposite term

$$\frac{1}{\rho_0} \int_0^H J(H, \rho) dz$$

(J is a Jacobi operator) responsible for the JEBAR, is unrealistically large.

We also examined the problem of velocity oscillations due to the numerical scheme. Our finite element numerical procedure may be treated for the case of uniform triangulation as some finite-difference scheme on the A-grid by Arakawa's classification. It is known that the A-grid schemes produce numerical noise. We may expect that, where the boundary condition for the velocity

$$u_n = 0 \quad \text{on } \Gamma_s,$$

is approximated in the horizontal plane by three-point correlation, this noise will be strongest in the areas of sharp coastline variations with intensive alongshore currents. To examine this assumption, we carried out numerical experiments with the minimal sea depth being limited to 50 m, which should reduce the JEBAR influence. All the passages were blocked, but there was baroclinicity and wind stress in the model. The result is presented in Fig. 1.5.

Here it is obvious that there are two-point oscillations at the side boundary, and these oscillations are most prominent at the corner points of the model area. Finite-difference schemes on the B and C grids do not produce such noise, because they perform, in essence, some spatial averaging over boxes (or their facets) which may also be treated as cubic finite elements. Consequently, we may consider the problem of a noisy velocity field to be one of interpretation of the results. The simplest way to filter noise is to average the results over four points. The result of filtering is presented in Fig. 1.6.

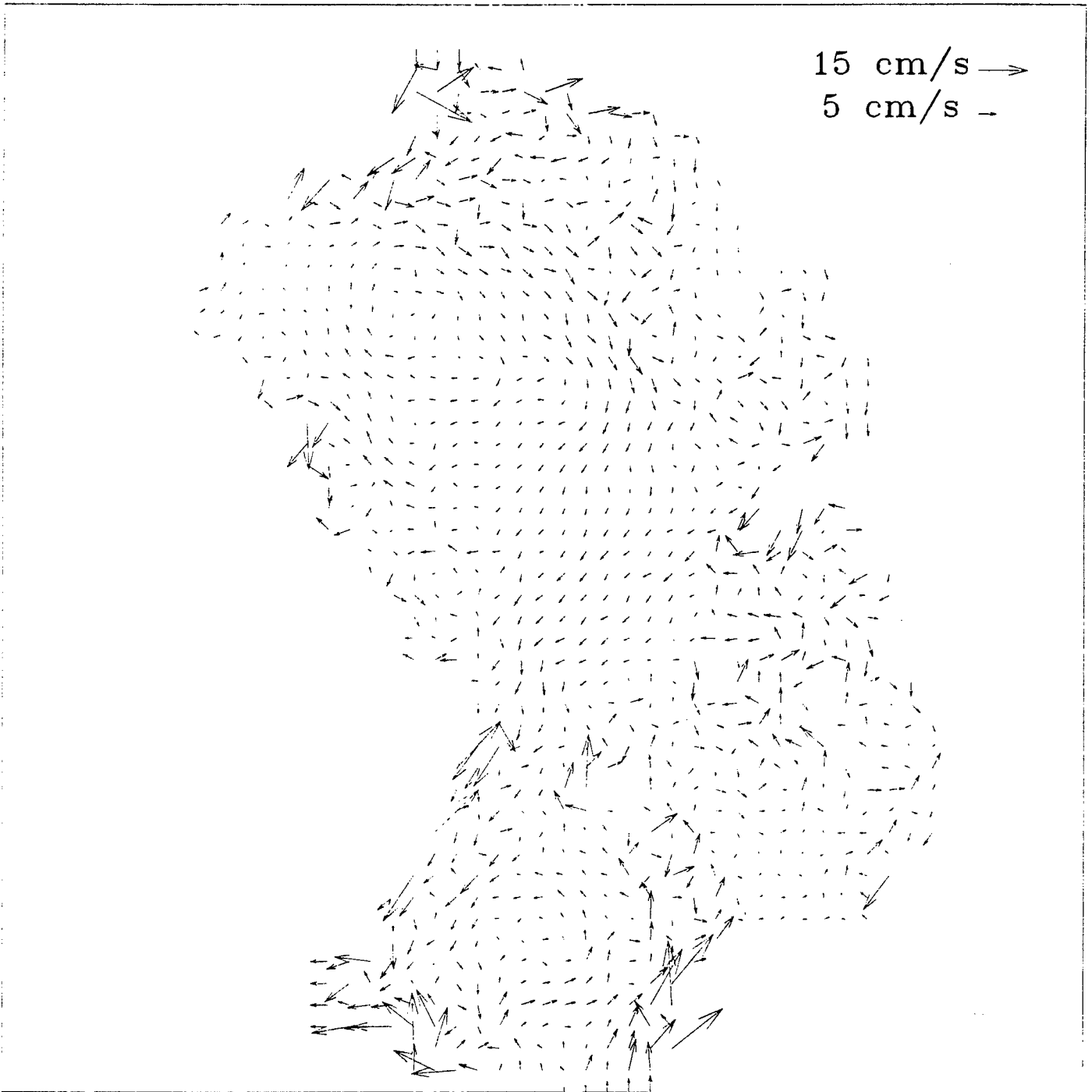


Fig. 1.3. Flow velocity at the 25m depth

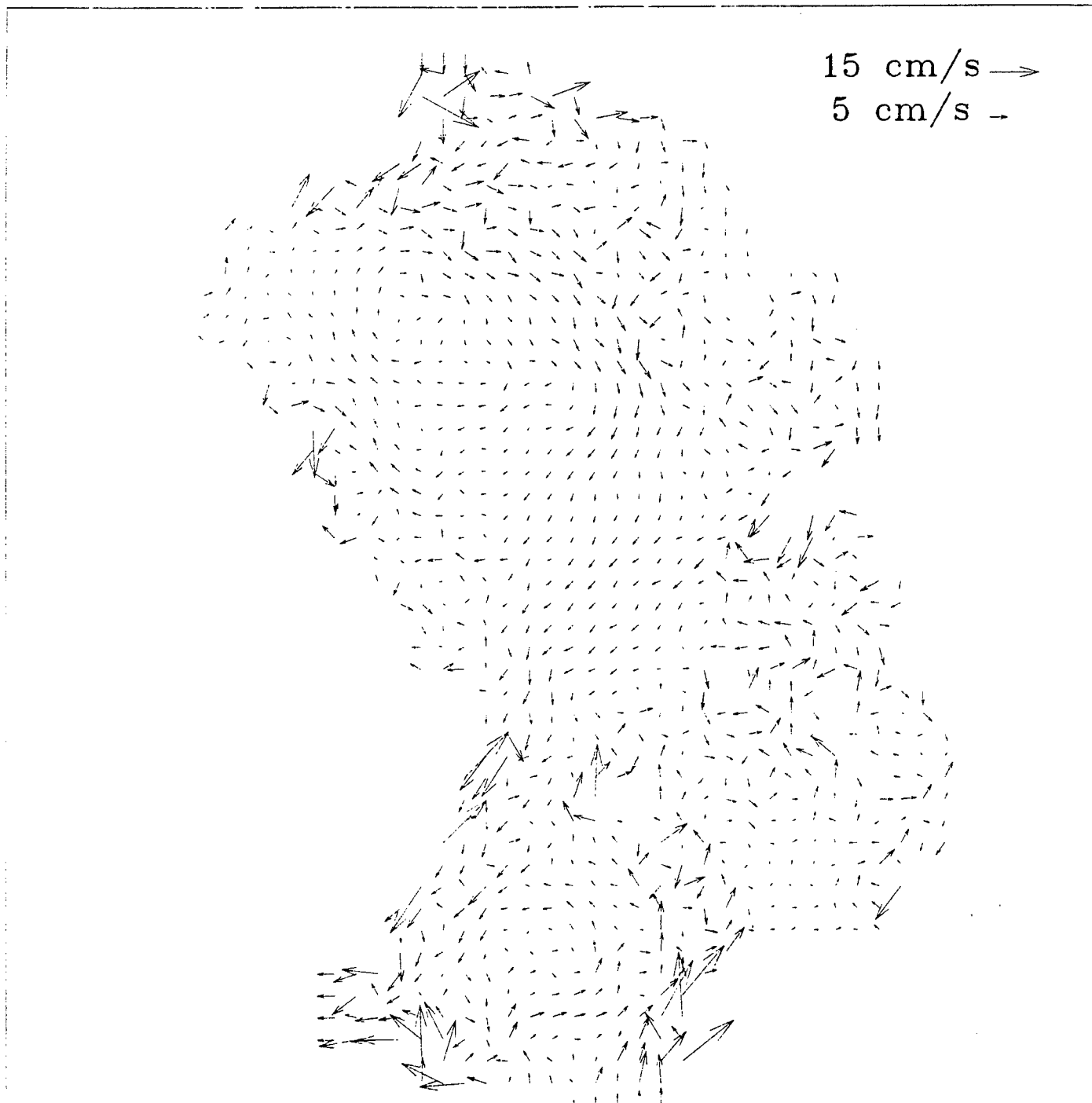


Fig. 1.4. Flow velocity at the 500m depth

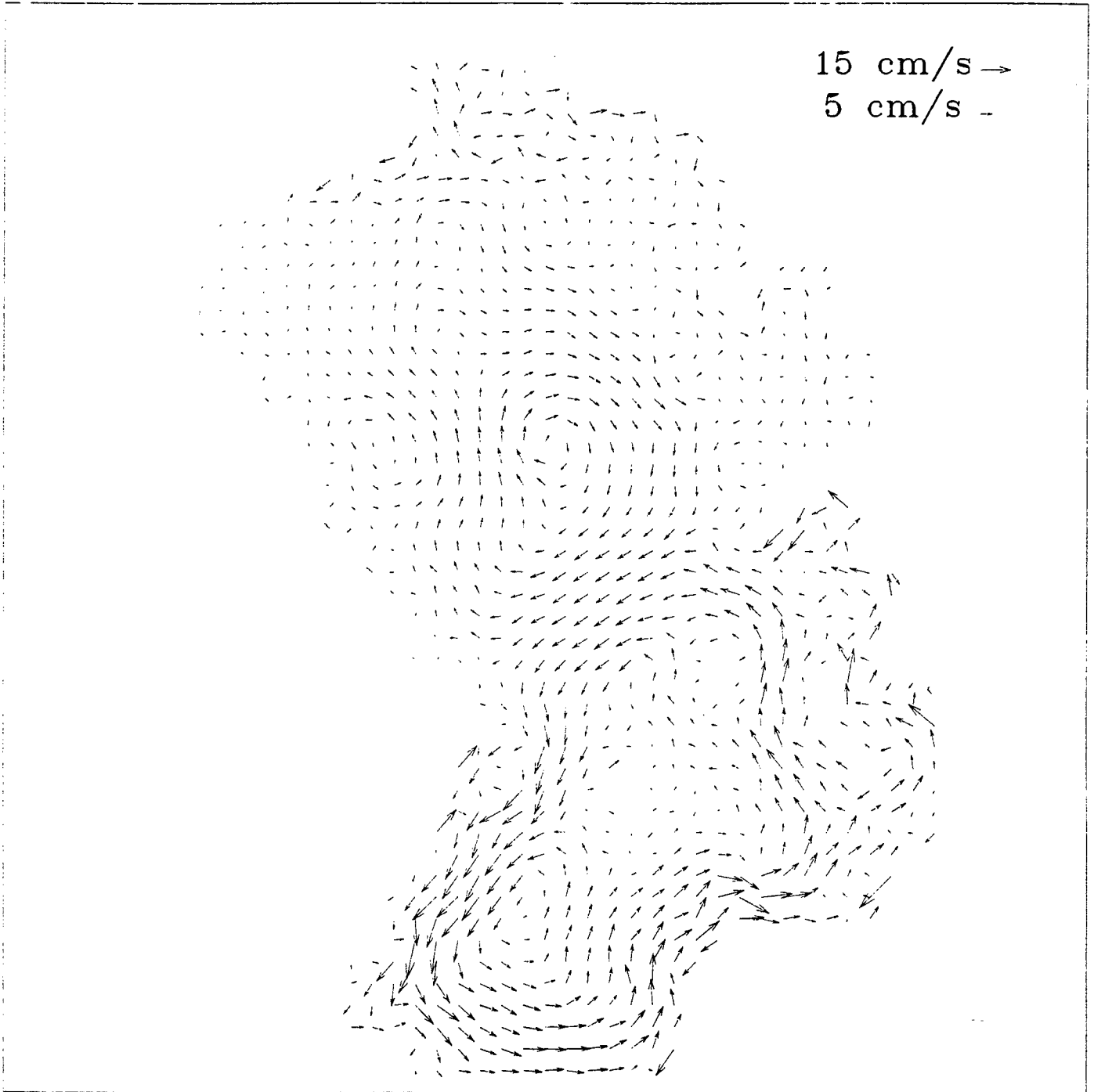


Fig. 1.5. Test for the velocity oscillations at the side boundary.

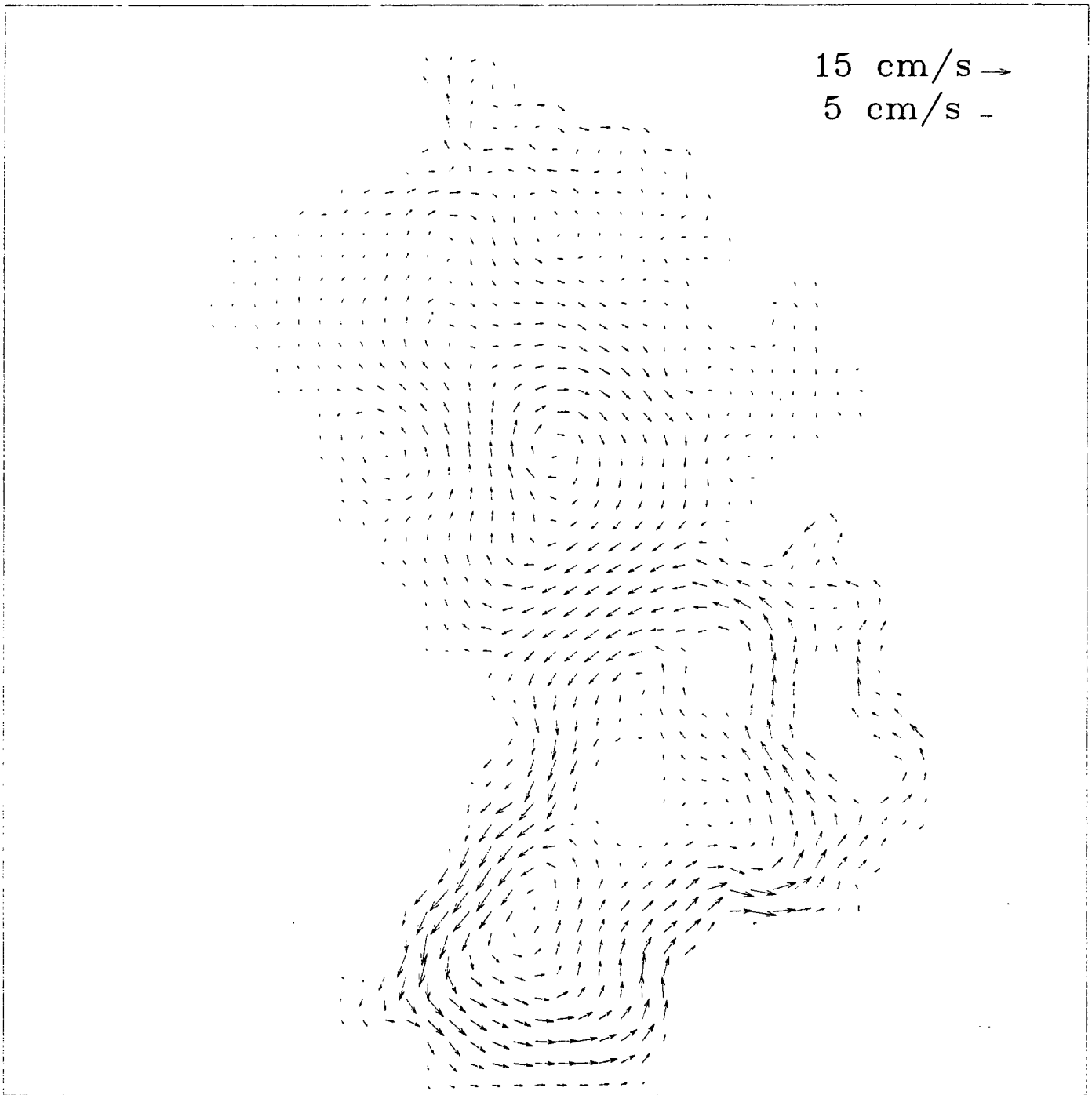


Fig. 1.6. Flow velocity averaged over four grid points.

1.2. Comments on the choice of turbulent mixing/diffusion coefficients

We used constant coefficients of turbulent mixing and diffusion in the general circulation model. Their values were as follows:

Horizontal mixing	$2 \cdot 10^8 \text{ m}^2\text{s}^{-1}$
Horizontal diffusion of T,S	$1 \cdot 10^7 \text{ m}^2\text{s}^{-1}$
Vertical mixing	$50 \text{ m}^2\text{s}^{-1}$
Vertical diffusion of T,S	$1 \text{ m}^2\text{s}^{-1}$

One may argue that these coefficients are very large. We gathered all available information on the coefficients used in other circulation models of the Arctic Ocean. The results of the investigation are summarized in Table 1.1. Because of poor information on the possible values of vertical coefficients, we outline only the horizontal coefficients.

Table 1.1. The coefficients of horizontal mixing in different models

Model and horizontal resolutions	Horizontal mixing	Recalculated values
Semjonov G., Russia 28 km - 312 km	Smagorinsky, $8 \cdot 10^6 - 9 \cdot 10^7 \text{ m}^2\text{s}^{-1}$	$10^8 - 10^9 \text{ m}^2\text{s}^{-1}$
Polyakov I., Russia 55.6 km	Constant $10^7 \text{ m}^2\text{s}^{-1}$	$4 \cdot 10^7 \text{ m}^2\text{s}^{-1}$
Hakkinen S., USA 28 km - 150 km	Constant $3 \cdot 10^7 \text{ m}^2\text{s}^{-1}$	$1.5 \cdot 10^7 \text{ m}^2\text{s}^{-1} - 3 \cdot 10^8 \text{ m}^2\text{s}^{-1}$

The first column shows the designer of the model and the horizontal spatial resolution used in the model. The second column shows the value (or the range of values) of the horizontal mixing coefficient. The third column shows the effective mixing coefficient recalculated for a horizontal resolution of 100 km. It is not very easy to compare these data, because the models are quite different with a lot of specific numerical features. In Semjonov's model, Smagorinsky's parameterization is used. Background mixing in the model is rather small, but depends heavily on the grid size and the velocity deformation. This mixing is very large near Greenland. Hakkinen's model uses very smooth fields of temperature and salinity, and even in this case, the mixing is close to the results of our model. Polyakov proposed, formally, the less viscous model. However, this model has "numerical" viscosity due to the first order schemes applied for advection. Thus, we may conclude that our model is comparable to other models for the Arctic Ocean.

II. CURRENT VERSION OF THE ARCTIC BASIN OCEANOGRAPHIC DATA BASE

2.1. Introduction

This section describes briefly the oceanographic data base collected to support the thinking on the evolution of large-scale anomalies in the Arctic Basin. This data base will be useful for many other investigations into Arctic Basin oceanography.

To begin with, the procedure of replacement of the CTD data in the Arctic part of the World Ocean Atlas - 1994 (WOA-94) is described. Then, the preliminary results of combining the Arctic Master Oceanographic Observation Data Set (MOODS) with the WOA-94, are given, and lastly, miscellaneous information concerning Arctic oceanographic data, presently available, is listed.

2.2. The new version of CTD data in the Arctic part of the WOA-94.

It is known that almost one third of all the WOA-94 CTD profiles were truncated due to a programming error. According to the NODC Internet information:

- this error resulted in reporting some of the CTD files to depths shallower than they were actually measured;
- this concerns the profiles in the CTD probe files only;
- the error has been corrected and new CTD files are currently available electronically and on CD-ROM;
- the new files include all the CTD profiles which previously contained errors as well as all the other profiles;
- the profile identification numbers (PINs) in these new files differ from the PINs on the WOA-94 CD-ROMs.

The WOA-94 data are organized by ten-degree latitude-longitude squares which are identical to those specified in the ten-degree square numbering scheme of the World Meteorological Organization (WMO). Within each of the WMO subdirectories there is a file containing the CTD profile data. Therefore, the ten-degree squares containing CTD files, were selected from the CD-ROM "Replacement CTD data" (version of 1996). These squares were: 1800, 1801, 7800, 7801, 7806, 7717, 7716, 7715, 7714, 7713, 1717. Then, all the CTD data located in the corresponding squares of the WOA-94, were chosen. It is necessary to note, that not all of the squares within the Arctic Basin are represented in the new version of the CTD files. We did not consider the squares corresponding to the Nordic seas, the Arctic seas, and the Canadian Arctic Archipelago (7701-7710 and 1701-1715).

To characterize the differences between the new and the old versions of the CTD profiles, three types of profiles were grouped (Table 2.1). The first type are profiles from different versions with similar country codes, expedition codes, dates, times, coordinates, equal or more numbers of measured characteristics in the new version, and with more numbers of measurement levels and deeper levels of the lowest levels of observations, in the new version. The second type

are profiles from different versions with similar country codes, expedition codes, dates, times, coordinates, lowest depths, and number of measured characteristics and levels, while the third type are of profiles from those different versions which are not included in groups 1 and 2.

Table 2.1. The distribution of the profiles of the CD-ROM "Replacement CTD data - 96" and the WOA-94.

Source and region	Number of profiles	Number of profiles in the first group	Number of PINs in the first group	Number of profiles in the second group	Number of PINs in the second group	Number of profiles in the third group	Number of PINs in the third group
1	2	3	4	5	6	7	8
Replacement CTD data; squares 1800, 1801, 7800, 7801, 7806	155	67	67	84	84	4	4
WOA-94; squares 1800, 1801, 7800, 7801, 7806	154	67	67	84	83	4	4
Replacement CTD data; squares - 1717, 7713, 7714, 7715, 7716, 7717.	1653	52	51	1545	1542	60	60
WOA-94; squares - 1717, 7713, 7714, 7715, 7716, 7717; *.CTD files	1653	52	52	1545	1541	60	60

Analysis of Table 2.1, and further examination, allowed us to conclude that:

- the new version of CTD profiles replaces the files with name *.CTD in the WOA-94, rather than those with name *.CTD2;
- in addition to the NODC information, we have found other differences between the new and the old profiles, besides the number of levels and the lowest depth of observations (see Table 2.1, column 8);
- in group 3 (column 8 of Table 2.1), the observation times for the old and new versions are different in the pairs of profiles with the same header and data;
- the new and old versions of the CTD files contain duplicates, when compared by country and expedition codes, times, dates, coordinates and numbers of measured characteristics (see differences between columns 3 and 4, 5 and 6 in Table 2.1), while there are differences in the data;
- about 20-25 % of the PINs are the same in both versions, but correspond to different CTD stations;

- the range of PINs in the new version of the CTD profiles is similar to that in the WOA-94; therefore, some confusion could arise if one were to substitute these CTD profiles into the WOA-94, using the new PINs for the comparison of the headers;
- the "Replacement CTD data" CD-ROM contains one more station than the WOA-94 (see Table 2.1, column 2); however, the temperature and salinity in this profile (PIN 101944) are not realistic.

Fortunately, the other errors in the WOA-94, detected by NODC, and listed on the Internet, do not concern the Arctic regions.

2.3. The preliminary results from combining the Arctic Master Oceanographic Observation Data Set and the World Ocean Atlas -1994

There are 9333 profiles of the Arctic Master Oceanographic Observation Data Set (MOODS) in the public domain. The World Ocean Atlas -1994 (WOA-94) contains 10366 profiles within the Arctic Basin margins (15°W-105°E 80°N; 105°E-110°E 79°N; 110°W-130°W 77.5°N; 130°W-140°W 78°N; 140°W-160°W 79.5°N; 160°W-170°W 77°N; 170°W-170°E 75°N; 150°E-170°E 71°N; 135°E-150°E 70°N; 130°E-135°E 71°N; 125°E-130°E 75°N; 115°E-125°E 78°N; 90°E-115°E 80.5°N; 15°E-90°E 82.5°N). The general information on field activity in the Arctic, has allowed us to assume that there are a lot of duplicates in these two data collections. Therefore, the comparison between the MOODS and the WOA-94 data was made before the merging of the data bases. The new version of the CTD files in the WOA-94 was used for the comparison.

The common parameters which compose the profile header in both the MOODS and the WOA-94 are: date (including day, month, year), time, coordinates, number of measured characteristics, and number of observation levels. The duplicates were determined as profiles with similar common header parameters, except for time. All the other profiles from the MOODS were specified as new for the joint data base (Table 2.2).

Table 2.2. The distributions of the profiles from the MOODS and the WOA-94.

MOODS areas	Number of profiles from MOODS	Number of profiles from WOA-94	Number of new profiles from MOODS
1	2	3	4
area 1; 70°N - 80°N, 130°W - 169°W.	6409	5388	3754
area 2, 80°N - 90°N, 40°E - 138° W.	1844	3925	955
area 3, 80°N - 90°N, 138°W - 140°E	111	68	47
area 4, 70°N - 80°N, 169°W - 175°E	764	376	534
area 5, 80°N - 90°N, 40°E - 140° E	205	108	135

We are planning to apply a more restrictive algorithm in the comparison of temperature and salinity values, to detect additional profiles in the MOODS which do not coincide with the profiles in the WOA-94.

2.4. The current content of the Arctic Basin Data Base

Our Arctic Basin Data Base is growing due not only to the combining of commonly recognized collections, and the results of recent expeditions, but digitizing of the historical Russian data, also provides our data base with additional information. For example, we have digitized the unpublished archive of P.P. Shirshov in the framework of this contract (see rows 17, 26-41 of Table 2.3).

Table 2.3. Miscellaneous information about the current content of the Arctic Basin Data Base

No.	Data description	Location, deg., min. or region	Date month., year	Number of real stations or modeled profiles
1	2	3	4	5
1	World Ocean Atlas (WOA) - 94	Arctic Basin	06.1905- 10.1990	more than 10000 sts.
2	The public domain of the Arctic Master Oceanographic Observation Data Set (MOODS)	Arctic Basin	07. 1905- 03.1995	9333 sts.
3	Ice Camp "Turpan" (Russia-USA)	83.17N - 83.35N 23.45E - 27.23E	04.1994	6 sts.
4	Ice Camp "Narwhal" (USA-Canada) (additional data from "Narwhal" are available on the INTERNET).	Lincoln Sea, 83.33N - 83.35N, 62.59W - 63.14 W	04.1994	19 sts.
5	"Oden-91", Swedish RV (only small part of observations)	83.33N - 83.35 N 27.38E - 27.58 E	08.1991	2 sts.
6	SCICEX-95, American submarine SSXCTD data (SAIC part of the observation).	section between 72N, 150W and 85N, 51E.	04.1995	63 sts.
7	Winter and Summer profiles of Climatic Fields in the Arctic Ocean (1994)	Arctic Basin		3339 profiles
8	"POLEX" - gridded data from Russian quasi-synoptic aircraft surveys of the Arctic Basin	tracks from point Barrow to 1)Svalbard, 2)Franz Josef Land, 3) Severnaya Zemlya and from the Lincoln Sea to 4) Svalbard and 5) Franz Josef Land	03-05 of 1955-56, 1973-79	711 profiles

9	Ice Camp Gator (the exact day and time of measurements are not available)	74N; 150W	04.1992	9 sts.
10	Rose/Red Ice Camp (the exact day and time of measurements is not available)	73N; 164W	04. 1986	5 sts.
11	Ice Camp SIMI (no salinity)	74N; 150W	04. 1994	7 sts.
12	Ice Camp FRAMIV (only SVPs)	83N; 16E	04. 1982	5 sts.
13	Ice Camp Tanya (Approximate location, time and date)	86.5N, 14W	04. 1986	1 sts.
14	Ice Camp Jerry and Shirley	Lincoln Sea	04.1988	16 sts.
15	"Polarstern" data (part of observations)	81N-83N; 30E - 43E	09.1983	22 sts.
16	"Polarstern" data, ARCTIS IV/3 expedition(part of observations)	81.2N- 86.0N; 20E - 30E	07 -08 1987	18 sts.
17	"North Pole -1", Russian drifting station	80.23N - 88.53 N, 06.15W - 23.48E	06.1937 - 12.1937	28 sts.
18	"North Pole -5", Russian drifting station (part of observations)	85.24N-86.46N, 82.23E-120.44E	11.1955 - 11.1956.	5 sts.
19	"North Pole-6", Russian drifting station (part of observations)	82.25N-86.31N, 53.40E-142.15E	06.1958 - 03.1959.	4 sts.
20	"North Pole-7", Russian drifting station (part of observations)	85.41N - 86.22N, 44.26W- 157.25W	01.1958 - 03.1959	3 sts.
21	"North Pole-13", Russian drifting station (main part of observations)	78.14N - 85.55N, 91.30E - 170.23E	05.1965 - 04.1966.	22 sts.
22	"H - 169", Russian aircraft (part of observations)	78.28N - 81.37N 176.44 - 179.12 E	04.1941	2 sts.
23	Some results of Russian aircraft expeditions	80.04N - 86.56N, 157.20W - 142.09E	04.-0.5 of 1948, 1949, 1950, 1955.	16 sts.
24	Russian expedition on drifting ice (small part of observations).	80.51 N 109.43 E	04.1951	1 sts.
25	"Fram", Norwegian RV (famous Nansen expedition; part of observations)	80.25N - 85.30 N 59.06E - 132.04 E	04.1894 - 11.1895	4 sts.
26	"Nautilus", American submarine (some of these data are in WOA-94)	80.31N - 81.59 N, 1.10E - 24.45E	08. - 09 1931	9 sts.
27	"Sedov", Russian RV (part of observations)	75N - 86N; 4E - 153.E	08.1929 - 12.1939	199 sts.
28	"Litke", Russian RV (small part of observations)	81.40N, 9.23E 81.11N, 94.55E	09.1955 09.1940	1 sts. 1 sts.
29	"Stalin", Russian RV (part of observations)	80.13N - 81.00N; 2E - 4E	12.1939 - 01.1940	2 sts.

30	"Ermak", Russian RV	79.07N - 81.27N; 4.40E - 20.05E	06- 08 1897	15 sts.
31	"Krasin", Russian RV	79.24N- 81.47 N; 9.40E - 45.00E	07 - 09 1928	31 sts.
32	"Maligin", Russian RV	81.37N - 82.24N; 51.54E - 62.20E	08 - 09 1932	7 sts.
33	"Rusanov", Russian RV	79.15N - 82.03N; 54.00E - 101.32E	08.1932 - 10.1936	11 sts.
34	"Taymir", Russian RV	79.03N - 79.58N; 76E - 102E;	08.-09. 1932	15 sts.
35	"Persey", Russian RV	80.00N - 80.01N; 3.03E - 10.35 E	08.1934	4 sts.
36	"Sadko", Russian RV	77.00N- 82.41N; 3.19E - 94.38E	08.1934 - 09.1936	101 sts.
37	"Sibirakov", Russian RV	79.16N - 80.17 N; 6.40E - 91.34E	09.1936 - 06.1939	5 sts.
38	"Nerpa", Russian RV	79.00N - 82.15N; 50.23E - 95.23E	08.1937 - 09.1940	44 sts.
39	"Belgica", RV	79.12N - 80.17N; 1.29E - 17.02E	06. - 07. 1905	13 sts.
40	"Farm", RV	79.10N - 80.16 N; 8.10E - 12.05E	07.- 08. 1910	10 sts.
41	"Veslemov", ? RV	79.05N - 80.39N; 7.01E - 17.14E	07. - 08. 1912	39 sts.

The Data Base described above, will be used for analysis of the evolution of large-scale anomalies in the Arctic Basin.

REFERENCES

- Marchuk. G.I. and V.I. Agoshkov (1981). *Introduction to projection-grid methods*. Nauka, Moscow (in Russian).
- Pacanowski, R.C. and S.G.H. Philander (1981). Parameterization of vertical mixing in numerical models of tropical oceans. *J. Phys. Oceanogr.*, **11**, 1443-1451.
- Sarkisyan, A.S. (1977). *Numerical Analysis and Forecast of Sea Currents*. Gidrometeo-izdat, Leningrad, (in Russian).
- Zienkiewicz, O.C. (1977). *The Finite Element Method, 3 ed.*, McGraw-Hill, New York.